International Journal of Heat and Mass Transfer 77 (2014) 928–939

Contents lists available at ScienceDirect

International Journal of Heat and Mass Transfer

journal homepage: www.elsevier.com/locate/ijhmt

Thermal–hydraulic performance of a novel shell-and-tube oil cooler with multi-fields synergy analysis

Jie Yang, Lei Ma, Jiaju Liu, Wei Liu *

School of Energy and Power Engineering, Huazhong University of Science and Technology, Wuhan 430074, China

ARTICLE INFO

Article history:
Received 4 January 2014
Received in revised form 4 March 2014
Accepted 6 June 2014
Available online 3 July 2014

Keywords:
Oil cooler
Shell-and-tube heat exchanger
Spiral tubes
Multi-field synergy principle

ABSTRACT

In the present paper, a novel shell-and-tube heat exchanger is proposed for the application of oil cooler. It is numerically investigated compared to a rod baffles shell-and-tube heat exchanger using the commercial software FLUENT 6.3 and GAMBIT 2.3. The results of heat transfer, flow characteristics, and comprehensive performance are analyzed for both tube-side and shell-side with verifications of correlations and experimental apparatus. For tube-side, the novel heat exchanger demonstrates evidently excellent overall performance; while for shell-side, the novel heat exchanger illustrates slightly lower comprehensive performance than the rod baffles one. The path lines, pressure field, and temperature field are analyzed and the multi-fields synergy principle is adopted to evaluate the synergy extent between velocity, temperature, and pressure fields.

1. Introduction

Shell-and-tube heat exchangers (STHXs) are widely used in the petro-chemical industry, manufacturing industry, food preservation, electrical power production and energy conservation systems, due to their structural simplicity, relatively low cost and design adaptability. According to Master and co-workers, they account for more than 35–40% of the heat exchangers used in global heat transfer processes [1]. The conventional heat exchangers with segmental baffles (STHXsSB) are one of the most commonly used exchangers in the practical application. However, they have the disadvantages of high pumping power, fouling problems in the dead zones, and induction vibration of tube bundles [2]. Therefore, it is of great significance to propose new heat exchangers in order to overcome the above-mentioned drawbacks.

Lots of novel structures [3–29] have been suggested to enhance heat transfer, reduce power consumption and increase cost-effectiveness for the past decades. Among the those new heat exchangers, the main concept is altering the shell-side flow from zigzag pattern to longitudinal or helical pattern to avoid the impact of tube bundles and reduce the relaminarization and recirculation flow. As a result, this flow pattern variation increases heat transfer area, compresses heat exchanger, and improves cost-efficiency. Although the open literature is replete of multifarious novel heat exchangers, it is difficult to apply one heat exchanger for all fields since each design contains certain disadvantages. Therefore investigating new heat transfer enhancement techniques and proposing novel design to increase thermal–hydraulic performance are still in demands.

Experiments can provide highly reliable measurements of thermal–hydraulic performance; however, experiments can be extremely expensive and time-consuming compared to computational fluid dynamics (CFD). For very complex flows, such as those prevailing in the rod-baffle shell-and-tube heat exchanger, selecting an appropriate modeling approach can be difficult. There are complex tradeoffs between accuracy and computational expense. For example, a heat exchanger with 500 heat transfer tubes and 10 baffles requires at least 150 million computational cells to resolve the geometry. So far there are four main modeling approaches used for numerical simulations: the unit model [30,31,20], the periodic model [32,33], the porous model [34–37,21] and the whole model [38–40]. Recently Yang et al. [41] summarized the four modeling approaches, conducted a comparison of four different models on numerical accuracy, grid system size, computational period, and restriction, and provided an approach on selecting the most appropriate model for the practical situation.

So far, the performance evaluation criteria (*PEC*) [42,43], efficiency evaluation criterion (*EEC*) [44,45], and multi-fields synergy principle [46–53] have been proposed to evaluate performance and effectiveness. They all have been successfully utilized to analyze thermal–hydraulic performance. Through a wide literature survey, it is noticed that little work about its application on the whole model simulation of a shell-and-tube heat exchanger have

* Corresponding author. Tel.: +86 27 87541998; fax: +86 27 87540724.
E-mail address: w_liu@hust.edu.cn (W. Liu).

http://dx.doi.org/10.1016/j.ijheatmasstransfer.2014.06.015
0017-9310/

Nomenclature

A_h	hydraulic area (m^2)
A	heat transfer area (m^2)
c_p	specific heat capacity (kJ kg^{-1} K^{-1})
$C_{1\varepsilon}$	empirical constant (–)
$C_{2\varepsilon}$	empirical constant (–)
C_μ	empirical constant (–)
D_i	tube inner diameter (m)
D_o	tube outer diameter (m)
D_s	shell inner diameter (m)
D_h	hydraulic diameter (m)
f	friction coefficient (–)
G_k	producing item of k by average velocity gradient (kg m^{-1} s^{-3})
h	heat transfer coefficient (W m^{-2} K^{-1})
i, j, k	component on x, y, z coordinates (–)
k	turbulent kinetic energy (m^2 s^{-2})
L	baffle pitch (mm)
L_0	baffle distance from head (mm)
L_t	tube length (m)
n	tube quantity (–)
Nu	Nusselt number (–)
PEC	performance evaluation criteria (–)
P_h	hydraulic length (m)
p_s	pitch of the helix curve (mm)
p	pressure (Pa)
ΔP	pressure drop (Pa)
Q	heat transfer power (W)
Re	Reynolds number (–)
S	eccentric distance (mm)
T	temperature (K)
u	inlet average velocity (m s^{-1})
U	flow velocity of fluid (m s^{-1})
r, θ, h	cylindrical coordinates (–)

Greek symbols

ρ	fluid density (kg m^{-3})
λ	thermal conductivity (W m^{-1} K^{-1})
μ	dynamic viscosity (kg m^{-1} s^{-1})
ε	turbulent dissipation rate (m^2 s^{-3})
σ_k	Prandtl numbers corresponded to k (–)
σ_ε	Prandtl numbers corresponded to ε (–)
β	synergy angle (°)
θ	synergy angle (°)

Subscripts

ave	average value
e	enhanced heat exchanger
p	primary heat exchanger
w	wall

been reported in open literature since these procedures consume too much computational resources. In this paper, a novel oil cooler is proposed to provide an alternative solution for industrial designers. 3-D numerical simulations of the heat exchanger for both tube-side and shell-side are developed. The thermal–hydraulic performances of tube-side and shell-side are investigated and *PEC* is used to analyze the results. The present work also extends the application of multi-fields synergy principle on the whole model simulation of shell-and-tube heat exchanger, thus filling the gap in open literature.

2. Model formulation

2.1. Geometric introduction

Recently our research group invented a novel heat transfer tube called *eccentric spiral tube* as shown in Fig. 1. Each cross section of the tube is a circle. The centerline of tube is a helix curve and its equation in cylindrical coordinate system is expressed as follows:

$$\begin{cases} r(t) = \left\{ \begin{array}{ll} \sin t \cdot s & 2\cdot(k-1)\cdot\pi \leqslant t \leqslant \frac{2k\pi}{4} \\ s & \frac{2k\pi}{4} \leqslant t \leqslant \frac{6k\pi}{4} \\ -\sin t\cdot s & \frac{6k\pi}{4} \leqslant t \leqslant 2k\pi \end{array} \right\} k \in Z \\ \theta(t) = t \\ h(t) = p_s \cdot t \end{cases} \quad (1)$$

where r, θ, h are the coordinates in cylindrical coordinate system; s stand for the eccentric distance of the tube centerline; p_s stands for the pitch of the helix curve; D_o and D_i represent the outer and inner diameter of tube cross-section, respectively. In the present work, D_o and D_i is set as 16 and 14 mm, p is set as 40 mm, s is set as 2.5 mm.

Motivated from the rod baffle heat exchanger [6–9] and twisted tubes heat exchanger [10–14], our research group proposed a novel shell-and-tube heat exchanger as shown in Figs. 2 and 3. The original plain tubes in the conventional STHXsSB are replaced by this novel heat transfer tubes. This alignment results in heat transfer tubes contacting at many points along the length of tube in bundle. So all tubes are tightly braced and there exists no tube movement during working condition. The spiral tubes are assembled into such a bundle that there is no need to install any baffles (segmental, helical, orifice, rod, trefoil-hole, or flower baffles) or supporting parts (ring) between each tube in the heat exchanger. Therefore, it is expected that this shell-and-tube heat exchanger with spiral tubes (STHXsST) has the advantages of higher thermal–hydraulic performance, higher thermal effectiveness, tube bundle vibration elimination, and lower fouling due to its unique structure in both tube-side and shell-side. As one of the most outstanding inventions in the field of shell-and-tube heat exchanger, the shell-and-tube heat exchanger with rod baffles (STHXsRB), rather than STHXsSB, is taken as the reference group in order to demonstrate the novelty and improvement of the new oil cooler. The optimized geometric parameters [54,55] are adopted in the present work as presented in Table 1. For STHXsRB and STHXsST, all geometric parameters including shell diameter, shell length, tube number, inlet and out-

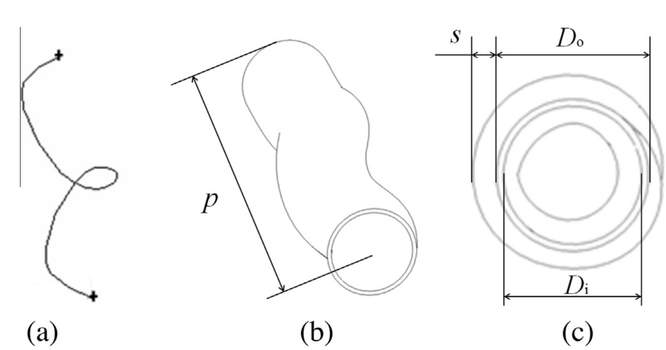

Fig. 1. Schematic diagram of the eccentric spiral tube: (a) the tube centerline; (b) the spiral tube; (c) the front view.

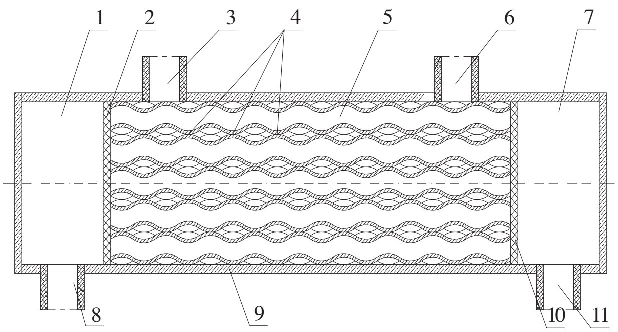

Fig. 2. 2-D diagram of the shell-and-tube heat exchanger with spiral tubes: 1. fluid cavity; 2. tube sheet; 3. shell-side inlet; 4. contacting points; 5. spiral tube; 6. shell-side outlet; 7. fluid cavity; 8. tube-side outlet; 9. shell wall; 10. tube sheet; 11. tube-side inlet.

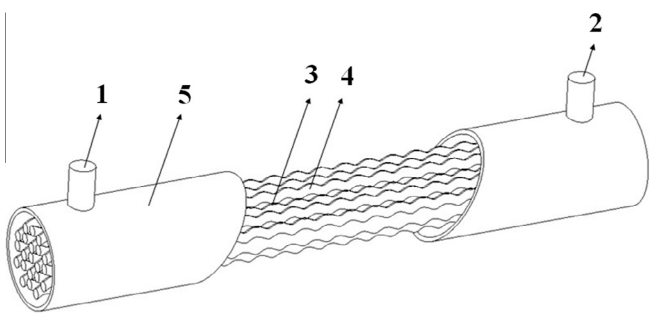

Fig. 3. 3-D diagram of the shell-and-tube heat exchanger with spiral tubes: 1. shell-side inlet; 2. shell-side outlet; 3. contacting points; 4. spiral tube; 5. shell-side outer wall.

Table 1
Structural parameter of shell-and-tube heat exchanger.

Shell diameter (D_s)	144 mm
Tube outer diameter	16 mm
Tube inner diameter	14 mm
Tube effective length	1000 mm
Tube pitch	22 mm
Tube number	21
Baffle number	7
Baffle thickness	5 mm
Baffle pitch (L)	120 mm
Baffle distance from head (L_0)	140 mm
Inlet and outlet nozzles	50 mm
Tube arrangement	Non-staggered placement

let nozzles are identical except the parameters involving configuration of spiral tube.

2.2. Governing equations, grid generation and boundary conditions

2.2.1. Governing equations

In the paper, the novel shell-and-tube heat exchanger is used as oil cooler, thus the fluid for tube-side is oil in laminar flow and fluid for shell-side is water in turbulent flow. The conservation equations for both fluids are presented in the tensor form in the Cartesian coordinate system as the flows are steady and the fluids are incompressible [56,57].

Continuity equation:

$$\frac{\partial u_j}{\partial x_j} = 0 \tag{2}$$

Momentum equation:

$$\rho \cdot \frac{\partial (u_i u_j)}{\partial x_j} = -\frac{\partial p_i}{\partial x_i} + \frac{\partial}{\partial x_j}\left(\mu\left(\frac{\partial u_i}{\partial x_j} + \frac{\partial u_j}{\partial x_i}\right)\right) \tag{3}$$

Energy equation:

$$\rho \cdot \frac{\partial (u_j T)}{\partial x_j} = \frac{\partial}{\partial x_j}\left(\frac{\lambda}{c_p}\frac{\partial T}{\partial x_j}\right) \tag{4}$$

where ρ is fluid density, λ is thermal conductivity, c_p is specific heat capacity, p is pressure, μ is dynamic viscosity, T is temperature. As the fluid for shell-side is in turbulent flow, the regular k–ε model is adopted:

Turbulent kinetic energy:

$$\rho \cdot \frac{\partial (k u_i)}{\partial x_i} = \frac{\partial}{\partial x_j}\left[\left(\mu + \frac{\mu_t}{\sigma_k}\right)\frac{\partial k}{\partial x_j}\right] + G_k - \rho\varepsilon \tag{5}$$

Turbulent energy dissipation:

$$\rho \cdot \frac{\partial (\varepsilon u_i)}{\partial x_i} = \frac{\partial}{\partial x_j}\left[\left(\mu + \frac{\mu_t}{\varepsilon_\varepsilon}\right)\frac{\partial \varepsilon}{\partial x_j}\right] + \frac{C_{1\varepsilon}\varepsilon}{k}G_k - C_{2\varepsilon}\rho\frac{\varepsilon^2}{k} \tag{6}$$

where k is turbulent kinetic energy, ε is turbulent dissipation rate, G_k is producing term of turbulent kinetic energy generated by mean velocity gradient, $C_{1\varepsilon}$ and $C_{2\varepsilon}$ are empirical constants, σ_k and σ_ε are Prandtl numbers corresponding to turbulent kinetic energy and turbulent dissipation rate, μ_t is defined as follows [56,57]:

$$\mu_t = \rho C_\mu \frac{k^2}{\varepsilon} \tag{7}$$

where $C_\mu = 0.09$, $C_{1\varepsilon} = 1.44$, $C_{2\varepsilon} = 1.92$, $\sigma_k = 1.0$, $\sigma_\varepsilon = 1.3$ and G_k is defined as follows [56,57]:

$$G_k = \mu_t\left(\frac{\partial u_i}{\partial x_j} + \frac{\partial u_j}{\partial x_i}\right)\frac{\partial u_i}{\partial x_j} \tag{8}$$

2.2.2. Grid generation

The geometric modeling and grid generation procedures were carried out with commercial CFD preprocessor GAMBIT 2.3. The 3D model is presented as in Fig. 3. According to the method given by Yang [41], the whole modeling approach is utilized for shell-side computational calculations as it provides the highest accuracy and real flow conditions while the other three modeling approaches cannot be used. The grid independence test was completed for each model. Taking the STHXsRB model as an example, five different grid systems with 5.0×10^6, 1.1×10^7, 1.7×10^7, 2.5×10^7 and 3.3×10^7 cells were adopted for calculation. The differences in heat transfer coefficient and friction coefficient between the third and fourth model are around 7% and the differences between the fourth and fifth model are around 2%. Thus, taking numerical resource cost and solution accuracy into consideration, the fourth model with 2.5×10^6 grid system was adopted. The model of STHXsRB was discretized with hexahedral meshes for the most flow region and with tetrahedral meshes for the baffle region, while the model of STHXsST was discretized with all hexahedral meshes. After the grid independence test, the final cell numbers for STHXsRB and STHXsST are 2.5×10^7 and 1.6×10^7, respectively. The meshes of heat exchanger models are shown in Figs. 4 and 5. For tube-side, hexahedral cells were adopted to mesh the internal space for the spiral tube. Local grid refinement was applied in the boundary layers. After grid independence test, the final cells number is around 2.5×10^6. The meshes of the spiral tube are shown in Fig. 6. All numerical calculations are

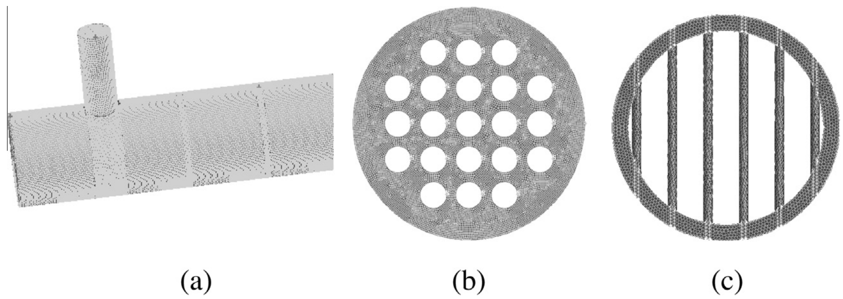

Fig. 4. Grid system of STHXsRB: (a) nozzles part; (b) front view; (c) rod baffle.

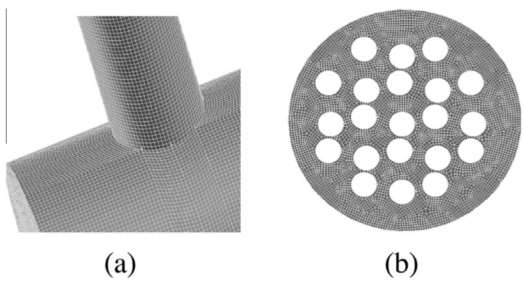

Fig. 5. Grid system of STHXsST: (a) nozzles part; (b) front view.

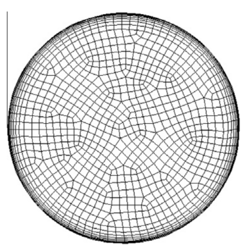

Fig. 6. Grid system of the spiral tube.

performed on a workstation with 20 dual-core CPUs and 160 GB RAM. Overall, it takes approximately 210 h to complete all calculations (not include the synergy angle calculations).

2.2.3. Boundary conditions

The commercial CFD software Fluent 6.3 was adopted for all the numerical simulations. The 3D, double-precision, pressure-based solver was used. The conservation equations are discretized with a finite volume formulation. The standard wall function method is adopted for the near-wall region, and a non-slip boundary condition is adopted on all solid surfaces. For shell-side the surfaces of solid regions are set as adiabatic because the impact caused by thermal conduction of the baffles can be neglected. The velocity-inlet boundary condition is applied for the inlet since for incompressible fluid the velocity-inlet boundary condition is equal to mass-flow-inlet boundary condition in Fluent, and the outflow boundary condition is applied for the outlet since the pressure for outlet is not given. The temperatures of tube inner and outer walls are set as constant and their values are taken from the average wall temperature determined in the experiments. The shell wall is set as adiabatic. The two-order upwind difference scheme is applied, and the SIMPLE algorithm is adopted for the coupling between pressure and velocity field; the two-order upwind difference scheme is applied for energy and momentum computation, and the standard difference scheme is used for the pressure. The other setting parameters adopt the default settings according to the user's guide in Fluent. The working fluids for shell-side and tube-side are set as water and oil and the corresponding parameters are listed in Table 2. The following assumptions are made to simplify numerical simulations for both tube-side and shell-side: the thermal-physical properties of the fluids such as ρ, μ, c_p, λ are constant; the working fluids are isotropic, Newtonian, incompressible, and continuous; the effect of gravity is negligible and viscous heating and thermal radiation are ignored.

2.3. Data reduction

The Reynolds number is expressed as follows:

$$\mathrm{Re} = \frac{\rho \cdot u \cdot D_h}{\mu} \tag{9}$$

where u is the fluid velocity, and D_h is the hydraulic diameter. For tube-side D_h is the inner diameter of tube, while for shell-side D_h is expressed as follows:

$$D_h = \frac{4A_h}{P_h} = \frac{\pi \cdot D_s^2 - \pi \cdot n \cdot D_o^2}{\pi \cdot D_s + \pi \cdot n \cdot D_o} \tag{10}$$

where A_h is the hydraulic area and P_h is the hydraulic length. D_s and D_o are inner diameter of shell and outer diameter of tube. n is the tube quantity. The Nusselt number is expressed as follows:

$$Nu = \frac{h \cdot D_h}{\lambda_f} \tag{11}$$

where λ_f is thermal conductivity and h is the convective heat transfer coefficient expressed as follows:

$$h = \frac{Q}{A \cdot (T_w - T_{ave})} \tag{12}$$

where Q is heat transfer power, A is heat transfer area, T_w is wall temperature and T_{ave} is average temperature for the working fluid. The friction factor is calculated as

$$f = \frac{2D_h \Delta P}{\rho L_t u^2} \tag{13}$$

where ΔP is pressure drop, L_t is tube length. The performance evaluation criteria are defined as following to measure the comprehensive performance [42,43]:

$$PEC = \frac{Nu_e/Nu_p}{(f_e/f_p)^{1/3}} \tag{14}$$

Table 2
Thermo-physical properties of fluid in oil cooler heat exchanger.

Parameters	Shell-side (water)	Tube-side (oil)
c_p (J/kg K)	4182	2270.1
μ (kg/m s)	0.001003	0.0095
ρ (kg/m^3)	998.2	826.1
λ (W/m K)	0.6	0.132

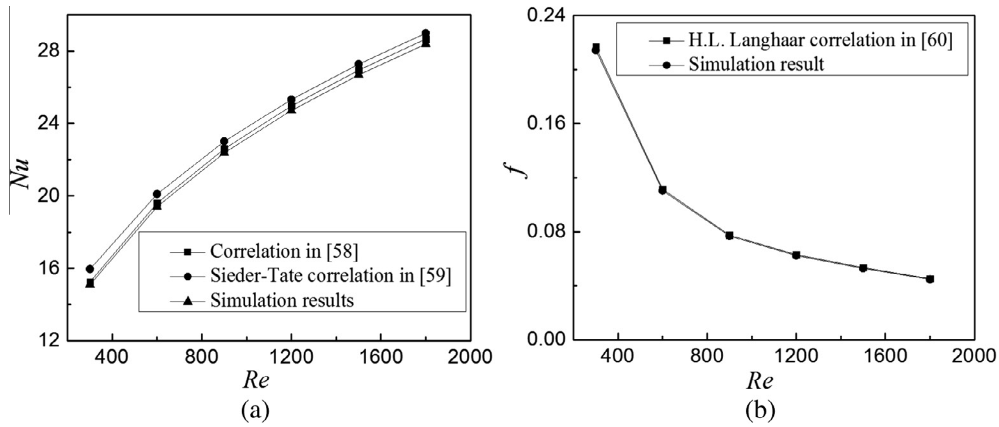

Fig. 7. Comparison between the simulation results and correlation results of plain tube: (a) *Nu*; (b) *f*.

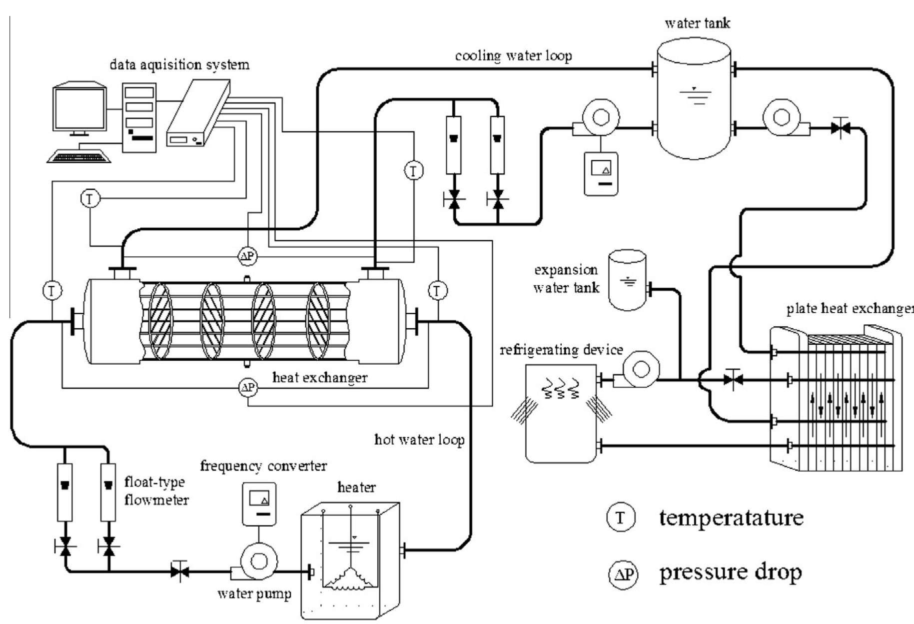

Fig. 8. Schematic diagram for experimental system.

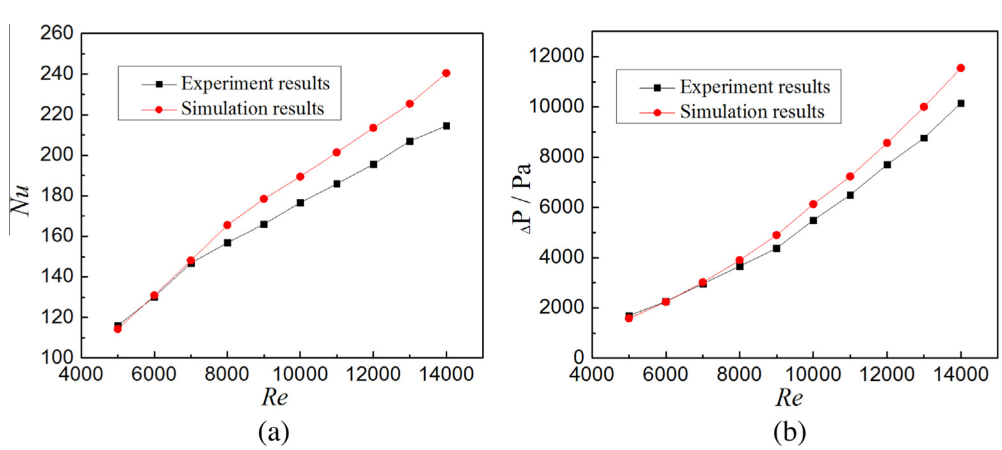

Fig. 9. Comparison between the simulation results and experimental results of shell-side for rod baffles heat exchanger [41].

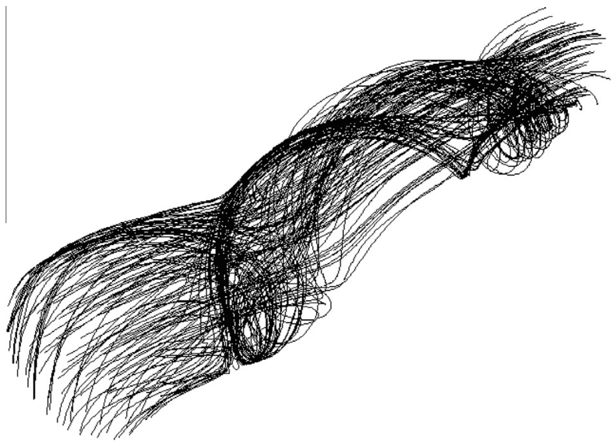

Fig. 10. The path lines in the spiral tube.

where the subscripts e stands for the enhanced heat exchanger and p stands for the primary heat exchanger.

3. Model validation

3.1. Tube-side

To verify the numerical modeling approach, the same modeling method was adopted for plain tube in laminar flow. The computational results were compared to the empirical correlations in literature [58–60]. For the laminar flow in a tube with entrance effect, the correlation in reference [58] was used to calculate Nusselt number expressed as follows:

$$Nu = 3.66 + \frac{0.065(D/L)\mathrm{Re}_D\mathrm{Pr}}{1 + 0.04[(D/L)\mathrm{Re}_D\mathrm{Pr}]^{2/3}} \tag{15}$$

and the Sieder–Tate correlation in Ref. [59] was also used to calculate Nusselt number expressed as follows:

$$Nu = 1.86\left(\frac{\mathrm{Re}_f\mathrm{Pr}_f}{l/d}\right)^{\frac{1}{3}}\left(\frac{\eta_f}{\eta_w}\right)^{0.14} \tag{16}$$

For the friction coefficient calculation, the H.L. Langhaar plot correlation was used to calculate friction coefficient. More information of the plot could be found in [60]. As shown in Fig. 7, it is seen that the CFD results and correlation outcomes are in good agreement. Therefore it is safely concluded that the tube-side model has a reliable accuracy.

3.2. Shell-side

In order to verify the precision of shell-side whole modeling approach on predicting heat transfer and pressure drop, experimental method was used. The schematic for the experimental system is presented in Fig. 8. The system consists of three loops, which are hot water loop, cooling water loop and refrigerating loop. The hot water loop contains a 58 kW electrical heater, water tank, hot water pump, flow meters and tube-side of a heat exchanger. The cooling water loop contains the water side of a plate heat

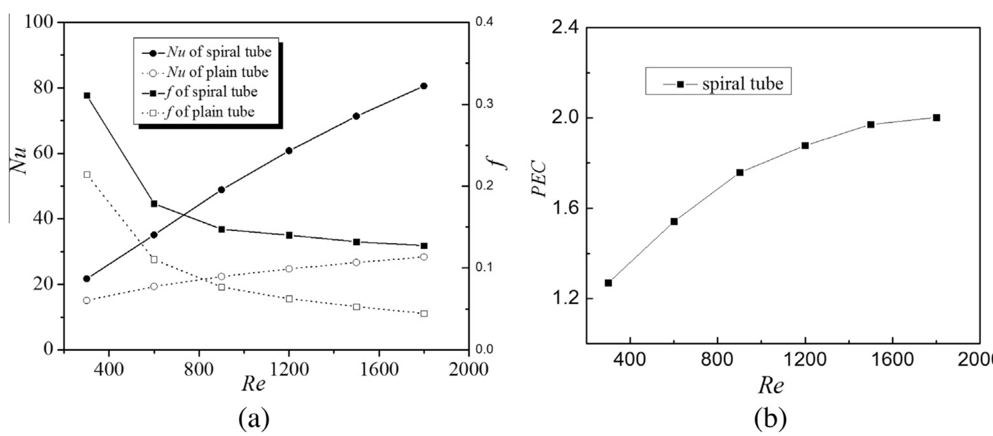

Fig. 11. Numerical results for spiral tube: (a) thermal–hydraulic performance; (b) performance evaluation criteria value.

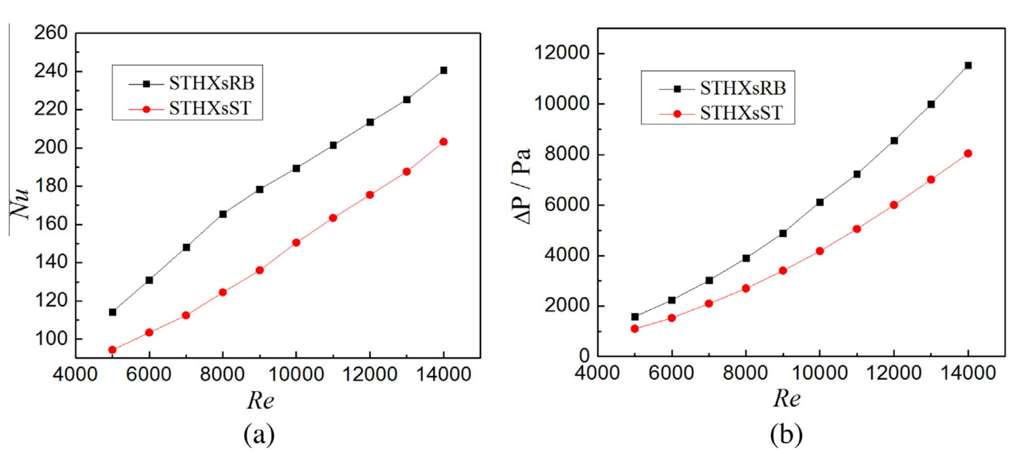

Fig. 12. Comparison between STHXsRB and STHXsST for shell-side: (a) Nusselt number; (b) pressure drop.

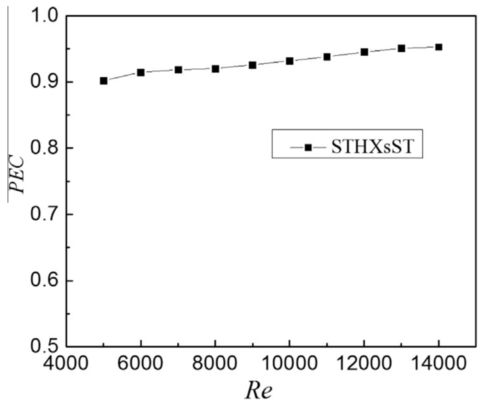

Fig. 13. The *PEC* value of STHXsST for different Reynolds number.

exchanger, water tank, cold water pump, flow meters and the shell-side of a heat exchanger. The refrigerating loop contains a 58 kW refrigerating unit device, pump and the refrigerant side of a plate heat exchanger. When the experiment is in steady operation, the heat generated by electrical heater is transferred from the hot water to the cold water in the heat exchanger. Then the thermal power in cooling water loop transfers heat from water to refrigerant at the plate heat exchanger. Finally, heat is rejected to ambient air. The volume flow rates for cold and hot fluids are measured using four rotary flow meters. The temperature of the fluids is measured using four K-type thermal couples that are inserted into holes at the hot fluid inlet, hot fluid outlet, cold fluid inlet, and cold fluid outlet. The pressure drops between inlet and outlet for the shell and the tube-side are measured using the two pressure drop transmitters. All data of temperature and pressure difference are transmitted in the PC system and automatically recorded through a data acquisition system. Due to the length limitation of context, more information regarding uncertainty analysis, data reduction and experimental apparatus could be found in [41] for reader's convenience.

Fig. 9 provides a comparison between numerical and experimental results for shell-side average Nusselt number and pressure drop for rod baffles heat exchanger [41]. It is observed that the

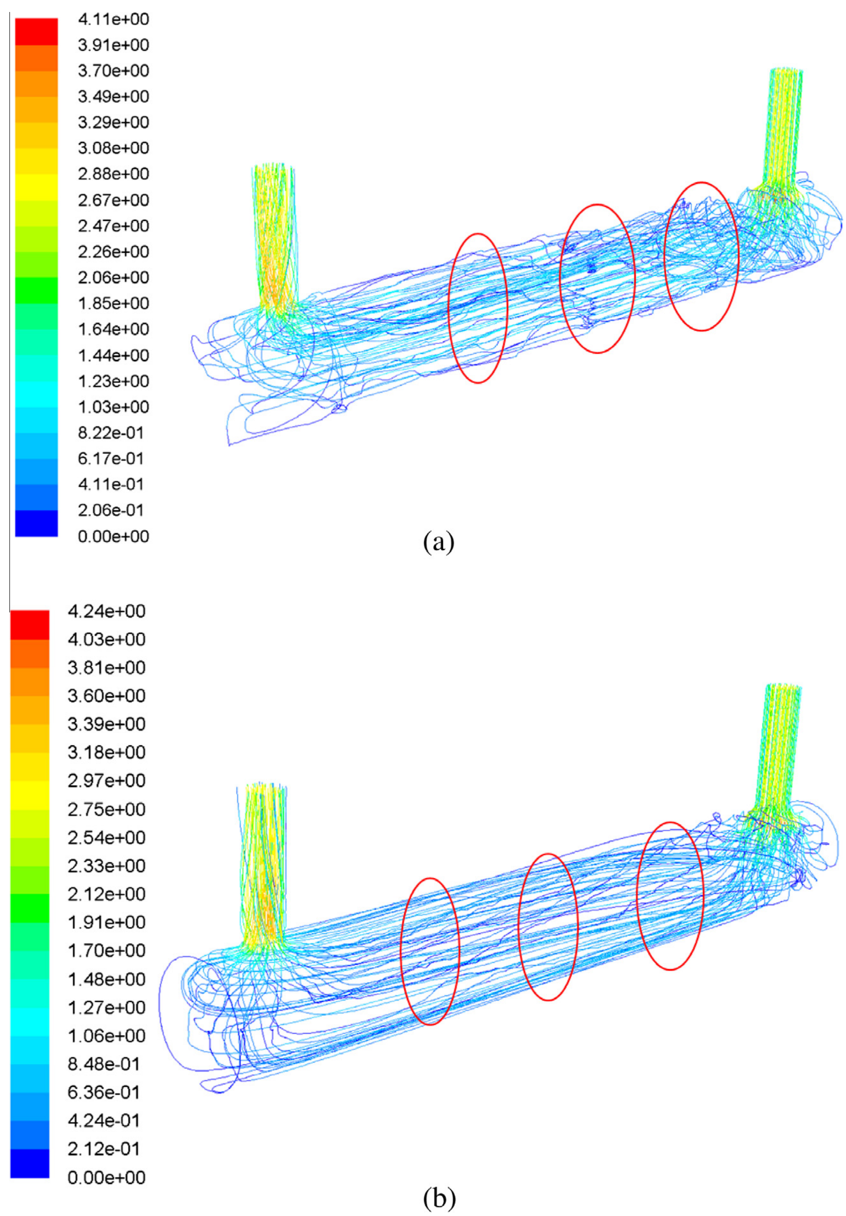

Fig. 14. Path lines in shell-side when Re = 14,000: (a) rod baffle heat exchanger; (b) heat exchanger with spiral tubes.

numerical results are in excellent agreement with experimental results. For most of the data points, the differences between computational and experimental results are less than 8%. The maximum discrepancies are about 10.8% for Nusselt number and 12.4% for pressure drop. Therefore it is decided that the whole modeling approach has a high precision on predicting thermal–hydraulic performance.

4. Analysis of thermal–hydraulic performance and discussion

To more clearly elucidate the underlying mechanism, the path lines in spiral tube are presented in Fig. 10. It is clearly seen that vortex has been formed near the wall of spiral tube, while the fluid in the core region can still maintain a straight bulk flow. The thermal–hydraulic performance and *PEC* are presented in Fig. 11. Fig. 11(a) shows that the Nusselt numbers of both spiral tube and plain tube increase with the increment of Reynolds number, while the former increases more rapidly. So the Nusselt number difference between spiral tube and plain tube increases with the increment of Reynolds number. Fig. 11(a) also depicts that all the friction coefficients decrease with the increment of the Reynolds number, and the spiral tube has larger friction factors than the plain tube. Fig. 11(b) demonstrates the comprehensive performance of spiral tube. It is seen that the *PEC* value increases with the increase of Reynolds number, ranging from around 1.25–2.1. So it is concluded that the spiral tube has obviously excellent overall performance than plain tube.

The comparison of the Nusselt numbers of shell-side for STHXsRB and STHXsST is presented in Fig. 12(a). It is clearly seen that the Nusselt number trends of all data are similar, that is, Nusselt number increases with Reynolds number. It can be seen that the Nusselt number of STHXsST is less than that of the STHXsRB. Quantitatively, the Nusselt number of STHXsST is approximately 75.1–85.4% that of STHXsRB. The comparison of the pressure drops of shell-side for STHXsRB and STHXsST is presented in Fig. 12(b). The variation trends of flow characteristics are in good agreement with the trends of Nusselt number, which increase with the increase of Reynolds number. The pressure drop of STHXsST is less than that of the STHXsRB. Quantitatively, the pressure drop of STHXsST is about 64.2–67.3% that of STHXsRB. For STHXsRB, the enhanced heat transfer performance is due to the mechanisms such as vortex and swirl flows and secondary circulations caused by the several arranged rod baffles along the flow direction, while

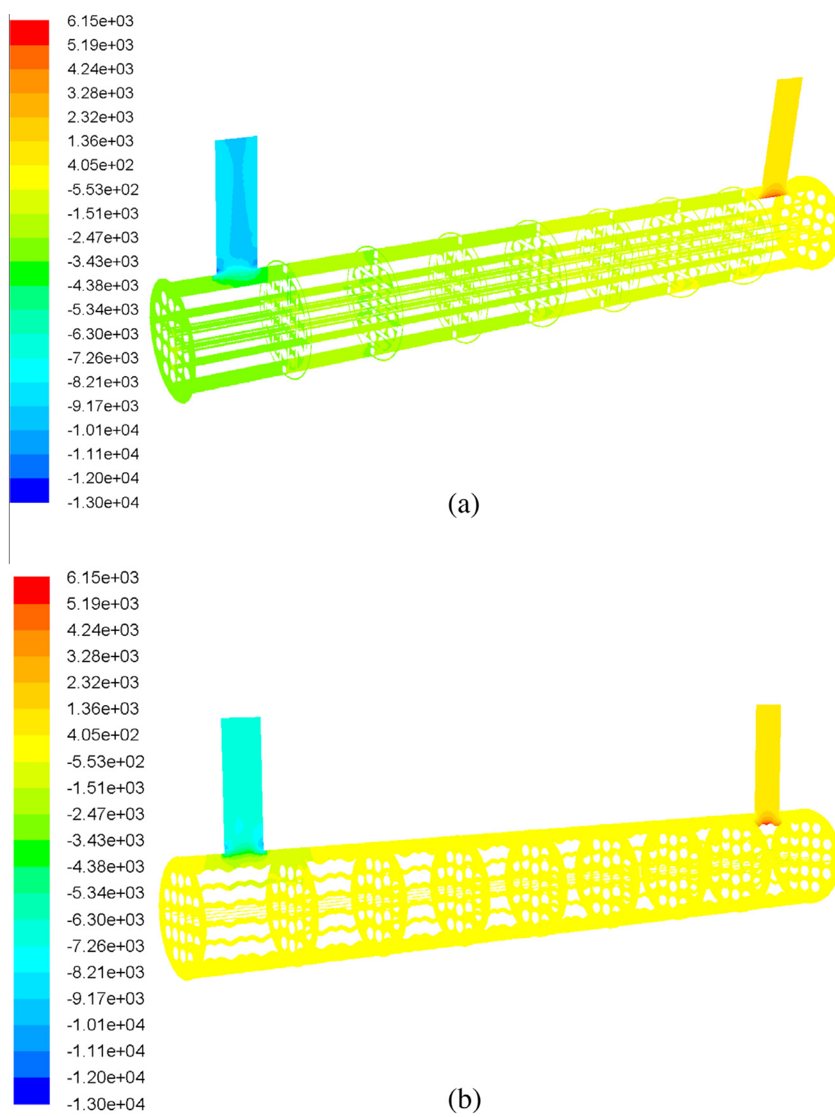

Fig. 15. Pressure distribution of shell-side when Re = 14,000: (a) rod baffle heat exchanger; (b) heat exchanger with spiral tubes.

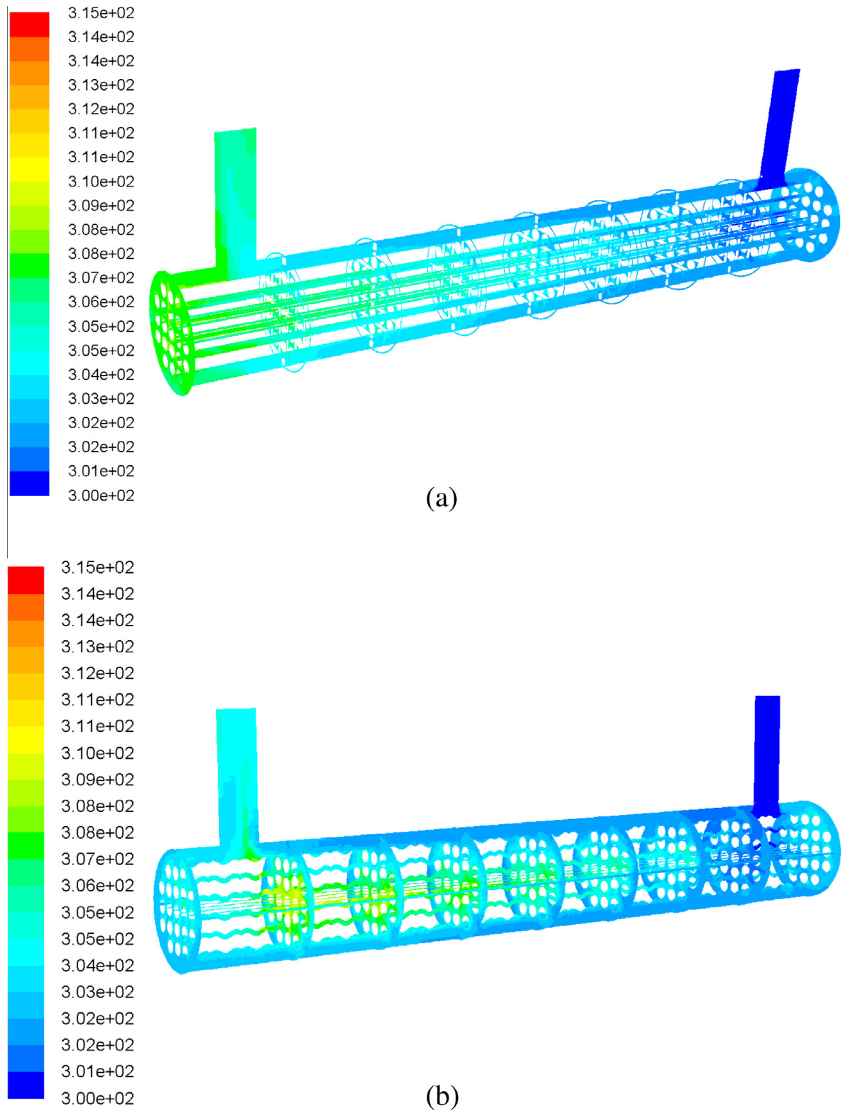

Fig. 16. Temperature distribution of shell-side when Re = 14,000: (a) rod baffle heat exchanger; (b) heat exchanger with spiral tubes.

for STHXsST the heat transfer is mainly due to the disruption and reattachment of boundary layers as the spiral tubes have the feature of curve surface. The relation of *PEC* value versus Reynolds number for STHXsST is presented in Fig. 13 in comparison with the primary heat exchanger, i.e. the rod baffle heat exchanger. It is observed that all *PEC* values of STHXsST exceed 0.9, revealing that the comprehensive performance of STHXsST is around ten percent less than that of STHXsRB according to performance evaluation criteria.

For the traditional shell-and-tube heat exchangers with segmental baffles, the shell-side flow is zigzag pattern. This flow pattern achieves enhancing heat transfer and pressure drop dramatically, but it yields many practical issues. It is well established from the open literature that altering the shell-side flow from zigzag pattern to longitudinal or helical pattern is a very promising design technique for shell-and-tube heat exchangers to overcome those real problems. It is easily expected that the shell flows in both STHXsRB and STHXsST are longitudinal, but the flow mechanisms are various, which will be validated in the following context. In conclusion, the shell-side overall performance of STHXsST is slightly lower than that of STHXsRB. But the tube-side overall performance is greatly better than that of STHXsRB. It also should be noticed that due to the unique configuration of spiral tube the heat transfer area of STHXsST is larger than that of STHXsRB, which results in larger area-volume ratio.

The path lines of shell-side for both heat exchangers when Reynolds number is 14,000 are shown in Fig. 14. It can be clearly seen that both flows are longitudinal and the flow in the shell-and-tube heat exchanger with spiral tubes is smoother than that of the rod baffles heat exchanger. Accompanying with the supporting rod baffles, the fluid flow is tortuous. The variation of shell-side fluid pressure is shown in Fig. 15. The streamwise decrease of fluid pressure is easily seen. It can be also observed that the pressure gradient for the shell-and-tube heat exchanger with spiral tubes is much smaller than that of the rod baffles heat exchanger. It is also seen that the pressure distribution for the novel oil cooler is more uniform than that of the old one. The variation of shell-side fluid temperature is shown in Fig. 16. It is seen that the temperature filed for the novel oil cooler is well-distributed along the shell-side.

5. Multi-fields synergy principle analysis

Guo [46], Tao [47], and Liu [48–53] proposed the multi-fields synergy principle and introduced several synergy angles, claiming

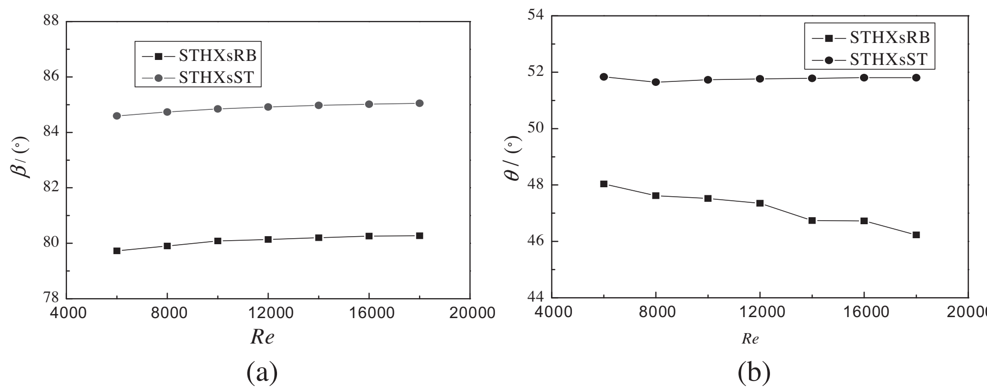

Fig. 17. Comparison of synergy angle β and θ between STHXsRB and STHXsST.

that they are relevant with the relations between velocity, temperature and pressure fields. The dot product of dimensionless velocity and temperature gradient in 2-D energy synergy equation can be expressed as [46]:

$$U \cdot \nabla T = |U||\nabla T| \cos \beta \tag{17}$$

Thus the synergy angle β is defined as follows:

$$\beta = \arccos \frac{U \cdot \nabla T}{|U||\nabla T|} \tag{18}$$

The synergy angle β between the temperature and velocity fields indicates the heat transfer enhancement extent for the novel techniques compared to the original heat transfer technique. Liu extended the synergy principles and proposed other synergy angles. The dot product of dimensionless velocity and pressure gradient in 2-D energy synergy equation can be expressed as [53]:

$$U \cdot (-\nabla p) = |U|| - \nabla p| \cos \theta \tag{19}$$

Thus the synergy angle θ is defined as follows:

$$\theta = \arccos \frac{U \cdot (-\nabla p)}{|U|| - \nabla p|} \tag{20}$$

The synergy angle θ between the pressure and velocity fields indicates the flow resistance variation for novel techniques compared to the original technique. According to the multi-fields synergy principle, the synergy angle β and θ is directly relevant to the heat transfer and hydraulic performance. After a wide range of literature review, little efforts of synergy field analysis on the whole shell-and-tube heat exchanger simulation have been reported. The main reason is that it takes a workstation with 160 GB RAM about 170 h to complete all the calculations for the shell-and-tube heat exchangers in this paper, so it would consume more time and computational resource to calculate synergy angle. In the present work, the synergy angles β and θ are calculated by a user defined function (UDF) program linked with FLUENT, as shown in Fig. 17.

According to the multi-fields synergy principle, it is expected that the synergy angle is consistent with Reynolds number as the flows in both heat exchanger are in full turbulence [44]. In Fig. 17(a), it is seen that synergy angle β vary little with Reynolds number for both STHXsRB and STHXsST which is in accordance with synergy principle. The synergy angle β for STHXsST is larger than that of STHXsRB for each data point demonstrating that the synergy extent between temperature and velocity fields for STHXsRB is better than that of STHXsST in turbulent flow. Quantitatively, the synergy angle β is 79.7–80.3° for STHXsRB and 84.9–85.3° for STHXsST. The original synergy angle β for the plain tube and heat exchangers without any baffles is expected to be 90° since the fluid velocity is perpendicular to the temperature gradient. The synergy degree between the temperature and velocity fields is intensified after adding the baffles parts or enhanced tubes, so the angle β will decrease correspondingly. In Fig. 17(b), the synergy angle θ varies little with Reynolds number for both STHXsRB and STHXsST as well. Although the synergy angle θ decreases slightly with Reynolds number, the angle difference between STHXsRB and STHXsST is larger than the variation. The synergy angle θ for STHXsRB is less than that of STHXsST for each data point illustrating that the synergy extent between pressure and velocity fields for STHXsST is better than that of STHXsRB in turbulent flow. Quantitatively, the synergy angle θ is 46.2–48.0° for STHXsRB and 51.6–51.8° for STHXsST. From the Figs. 12–14, it is concluded that the thermal–hydraulic performances are in consistence with multi-field synergy principle for the two heat exchangers.

6. Conclusions

(1) A novel shell-and-tube oil cooler was proposed and the CFD model was developed. The thermal–hydraulic performances for tube-side and shell-side were both investigated. The whole modeling approach was successfully applied for the new shell-and-tube heat exchanger.
(2) The *PEC* value for spiral tube is around 1.2 to 2.0, demonstrating that the shell-and-tube heat exchanger with spiral tubes has a better performance than the rod baffles shell-and-tube heat exchanger in tube-side. The *PEC* value for shell-side is around 0.9, illustrating that STHXsST has slightly lower performance than STHXsRB. Another advantage for STHXsST is that it possesses larger heat transfer area, leading to a more compact shell-and-tube heat exchanger. Therefore it is safe to draw the conclusion that the novel oil cooler provides a good alternative solution for industrial designers.
(3) The path lines, pressure distribution, and temperature distribution were numerically analyzed. The multi-fields synergy principle was implemented in the whole shell-and-tube heat exchanger simulation. It was used to evaluate and validate the novel heat exchangers from the perspective of the velocity, temperature and pressure fields. The whole shell-and-tube heat exchanger synergy angle calculations were performed thus filling the existing gap in the open literature.

Conflict of interest

None declared.

Acknowledgments

This work is supported by the National Natural Science Foundation of China (No. 51036003) and the National Key Basic Research Development Program of China (No. 2013CB228302).

References

[1] B.I. Master, K.S. Chunangad, V. Pushpanathan, Fouling mitigation using helixchanger heat exchangers, in: Proceedings of the ECI Conference on Heat Exchanger Fouling and Cleaning: Fundamentals and Applications, Santa Fe, USA, 2003, pp. 317–322.
[2] K.J. Bell, Delaware method for shell side design, in: S. Kakac, A.E. Bergles, F. Mayinger (Eds.), Heat Exchangers: Thermal–Hydraulic Fundamentals and Design, McGraw-Hill, New York, 1981, pp. 145–166.
[3] R. Mukherjee, Use double-segmental baffles in shell-and-tube heat exchangers, Chem. Eng. Prog. 88 (1992) 47–52.
[4] R. Mukherjee, Effectively design shell-and-tube heat exchangers, Chem. Eng. Prog. 94 (1998) 21–37.
[5] P.S. Williams, J.G. Knudsen, Local rates of heat transfer and pressure losses in the vicinity of annular orifices, Can. J. Chem. Eng. 41 (1963) 56–61.
[6] M.S. William, Angular rod baffle, U.S. Patent 4,127,165, Issued November 28, 1978.
[7] C.C. Gentry, Rod baffle heat exchanger technology, Chem. Eng. Prog. 86 (1990) 48–57.
[8] C.C. Gentry, Rod baffle heat exchanger, Appl. Therm. Eng. 18 (1998) VII–VIII.
[9] C.C. Gentry, ROD baffle heat exchanger design and application, in: Proceedings of the Tenth International Heat Transfer Conference: Heat Transfer, Brighton, UK, 1994, pp. 137–142.
[10] Brown Fintube Corporation, Twisted tube does more in the same space, Chem. Eng. Prog. 92 (1996) 9.
[11] D. Butterworth, Developments in shell and tube exchangers, in: International Center for Heat and Mass Transfer ICHMT International Symposium on New Developments in Heat Exchangers, Lisbon, Portugal 1993, pp. 6–9.
[12] X.H. Tan, D.S. Zhu, G.Y. Zhou, L.D. Zeng, Heat transfer and pressure drop performance of twisted oval tube heat exchanger, Appl. Therm. Eng. 50 (2013) 374–383.
[13] X.H. Tan, D.S. Zhu, G.Y. Zhou, L. Yang, 3D numerical simulation on the shell side heat transfer and pressure performances of twisted oval tube heat exchanger, Int. J. Heat Mass Transfer 65 (2013) 244–253.
[14] X.H. Tan, D.S. Zhu, G.Y. Zhou, L.D. Zeng, Experimental and numerical study of convective heat transfer and fluid flow in twisted oval tube, Int. J. Heat Mass Transfer 55 (2012) 4701–4710.
[15] J. Lutcha, J. Nemcansky, Performance improvement of tubular heat exchangers by helical baffles, Chem. Eng. Res. Des. 68 (1990) 263–270.
[16] D. Karl, P. Stehlik, R.J. Ploeg, B.I. Master, Helical baffles shell-and-tube heat exchangers, part 1: experimental verification, Heat Transfer Eng. 17 (1996) 93–101.
[17] P. Stehlik, J. Nemcansky, D. Karl, L.W. Swanson, Comparison of correction factors for shell-and-tube heat exchangers with segmental or helical baffles, Heat Transfer Eng. 15 (1994) 55–65.
[18] X. Xiao, L. Zhang, X. Li, B. Jiang, X. Yang, Y. Xia, Numerical investigation of helical baffles heat exchanger with different Prandtl number fluids, Int. J. Heat Mass Transfer 62 (2013) 434–444.
[19] X.H. Deng, S.J. Den, Investigation of heat transfer enhancement of roughened tube bundles supported by ring or rod supports, Heat Transfer Eng. 19 (1998) 21–27.
[20] Y.H. You, A.W. Fan, X.J. Lai, S.Y. Huang, W. Liu, Experimental and numerical investigations of shell-side thermo-hydraulic performances for shell-and-tube heat exchanger with trefoil-hole baffles, Appl. Therm. Eng. 50 (2013) 950–956.
[21] Y.H. You, A.W. Fan, S.Y. Huang, W. Liu, Numerical modeling and experimental validation of heat transfer and flow resistance on the shell side of a shell-and-tube heat exchanger with flower baffles, Int. J. Heat Mass Transfer 55 (2012) 7561–7569.
[22] Y.S. Wang, Z.C. Liu, S.Y. Huang, W. Liu, W.W. Li, Experimental investigation of shell-and-tube heat exchanger with a new type of baffles, Heat Mass Transfer 47 (2011) 833–839.
[23] S.B. Genic, B.M. Jacimovic, M.S. Jaric, N.J. Budimir, M.M. Dobrnjac, Research on the shell-side thermal performances of heat exchangers with helical tube coils, Int. J. Heat Mass Transfer 55 (2012) 4295–4300.
[24] A.W. Fan, J. Deng, J. Guo, W. Liu, A numerical study on thermo-hydraulic characteristics of turbulent flow in a circular tube fitted with conical strip inserts, Appl. Therm. Eng. 31 (2011) 2819–2828.
[25] X.Y. Zhang, Z.C. Liu, W. Liu, Numerical studies on heat transfer and flow characteristics for laminar flow in a tube with multiple regularly spaced twisted tapes, Int. J. Therm. Sci. 58 (2012) 157–167.
[26] Y.H. You, A.W. Fan, W. Liu, S.Y. Huang, Thermo-hydraulic characteristics of laminar flow in an enhanced tube with conical strip inserts, Int. J. Therm. Sci. 61 (2012) 28–37.
[27] A.W. Fan, J.J. Deng, A. Nakayama, W. Liu, Parametric study on turbulent heat transfer and flow characteristics in a circular tube fitted with louvered strip inserts, Int. J. Heat Mass Transfer 55 (2012) 5205–5213.
[28] X.Y. Zhang, Z.C. Liu, W. Liu, Numerical studies on heat transfer and friction factor characteristics of a tube fitted with helical screw-tape without core-rod inserts, Int. J. Heat Mass Transfer 60 (2013) 490–498.
[29] J. Guo, Y.X. Yan, W. Liu, F.M. Jiang, A.W. Fan, Effects of upwind area of tube inserts on heat transfer and flow resistance characteristics of turbulent flow, Exp. Therm. Fluid Sci. 48 (2013) 147–155.
[30] Q.W. Dong, Y.Q. Wang, M.S. Liu, Numerical and experimental investigation of shell-side characteristics for ROD baffle heat exchanger, Appl. Therm. Eng. 28 (2008) 651–660.
[31] W. Liu, Z.C. Liu, Y.S. Wang, S.Y. Huang, Flow mechanism and heat transfer enhancement in longitudinal-flow tube bundle of shell-and-tube heat exchanger, Sci. China Ser. E 52 (2009) 2952–2959.
[32] Y.G. Lei, Y.L. He, R. Li, Y.F. Gao, Effects of baffle inclination angle on flow and heat transfer of a heat exchanger with helical baffles, Chem. Eng. Process. 47 (2008) 2336–2345.
[33] J.F. Zhang, Y.L. He, W.Q. Tao, 3D numerical simulation on shell-and-tube heat exchangers with middle-overlapped helical baffles and continuous baffles-part II: simulation results of periodic model and comparison between continuous and noncontinuous helical baffles, Int. J. Heat Mass Transfer 52 (2009) 5381–5389.
[34] M. Prithiviraj, M.J. Andrews, Three dimensional numerical simulation of shell-and-tube heat exchanger, part II: heat transfer, Numer. Heat Transfer A-Appl. 33 (1998) 817–828.
[35] W.T. Sha, C.J. Yang, T.T. Kao, S.M. Cho, Multidimensional numerical modeling of heat exchangers, J. Heat Transfer 104 (1982) 417–425.
[36] Y.L. He, W.Q. Tao, B. Deng, X. Li, Y. Wu, Numerical simulation and experimental study of flow and heat transfer characteristics of shell side fluid in shell-and-tube heat exchangers, in: Proceedings of Fifth International Conference on Enhanced, Compact and Ultra-Compact Heat Exchangers: Science, Engineering and Technology, Engineering Conferences International, Hoboken, USA, 2005, pp. 29–42.
[37] Y.L. Shi, J.J. J, C.L. Zhang, Semiporous media approach for numerical simulation of flow through large-scale sparse tubular heat exchanger, HVAC&R Res. 16 (2010) 617–628.
[38] Z.G. Zhang, D.B. Ma, X.M. Fang, X.N. Gao, Experimental and numerical heat transfer in a helically baffled heat exchanger combined with one three-dimensional finned tube, Chem. Eng. Process. 47 (2008) 1738–1743.
[39] J.F. Zhang, Y.L. He, W.Q. Tao, 3D numerical simulation on shell-and-tube heat exchanger with middle-overlapped helical baffles and continuous baffles-part I: numerical model and results of whole heat exchanger with middle-overlapped helical baffles, Int. J. Heat Mass Transfer 52 (2009) 5371–5380.
[40] E. Ozden, I. Tari, Shell side CFD analysis of a small shell-and-tube heat exchanger, Energy Convers. Manage. 51 (2010) 1004–1014.
[41] J. Yang, L. Ma, J. Bock, A.M. Jacobi, W. Liu, A comparison of four numerical modeling approaches for enhanced shell-and-tube heat exchangers with experimental validation, Appl. Therm. Eng. 65 (2014) 369–383.
[42] R.L. Webb, Principles of Enhanced Heat Transfer, first ed., Wiley, New York, 1994.
[43] R.L. Webb, Performance evaluation criteria for use of enhanced heat transfer surfaces in heat exchanger design, Int. J. Heat Mass Transfer 24 (1981) 715–726.
[44] L. Ma, J. Yang, W. Liu, Physical quantity synergy analysis and efficiency evaluation criteria of convective heat transfer enhancement, in: Proceeding of IWHT International Workshop on Heat Transfer Advances for Energy Conservation and Pollution Control, Xi'an, China, 2011, pp. 1–11.
[45] L. Ma, J. Yang, W. Liu, X.Y. Zhang, Physical quantity synergy analysis and efficiency evaluation criterion of heat transfer enhancement, Int. J. Therm. Sci. 80 (2014) 23–32.
[46] Z.Y. Guo, W.Q. Tao, R.K. Shah, The field synergy (coordination) principle and its applications in enhancing single phase convective heat transfer, Int. J. Heat Mass Transfer 48 (2005) 1797–1807.
[47] W.Q. Tao, Y.L. He, Q.W. Wang, A unified analysis on enhancing single phase convective heat transfer with field synergy principle, Int. J. Heat Mass Transfer 45 (2002) 4871–4879.
[48] W. Liu, K. Yang, Mechanism and numerical analysis of heat transfer enhancement in the core flow along a tube, Sci. China Ser. E 51 (2008) 1195–1202.
[49] W. Liu, K. Yang, Z.C. Liu, Mechanism of heat transfer enhancement in the core flow of a tube and its numerical simulation, Open Transport Phenom. J. 2 (2010) 9–15.
[50] W. Liu, Z.C. Liu, S.Y. Huang, Physical quantity synergy in the field of turbulent heat transfer and its analysis for heat transfer enhancement, Chin. Sci. Bull. 55 (2010) 2589–2597.
[51] W. Liu, Z.C. Liu, L. Ma, Application of a multi-field synergy principle in the performance evaluation of convective heat transfer enhancement in a tube, Chin. Sci. Bull. 57 (2012) 1600–1607.
[52] W. Liu, Z.C. Liu, Z.Y. Guo, Physical quantity synergy in laminar flow field of convective heat transfer and analysis of heat transfer enhancement, Chin. Sci. Bull. 52 (2009) 3579–3586.
[53] W. Liu, Z.C. Liu, T.Z. Ming, Physical quantity synergy in laminar flow field and its application in heat transfer enhancement, Int. J. Heat Mass Transfer 52 (2009) 4669–4672.
[54] L. Ma, Y.S. Wang, J. Yang, Z.C. Liu, W. Liu, Numerical simulation of Rod Baffle heat exchangers and its optimum design, J. Eng. Thermophys. 32 (2011) 462–464 (in Chinese).

[55] L. Ma, Y.S. Wang, J. Yang, Z.C. Liu, W. Liu, Flow and heat transfer analysis of ROD Baffle heat exchangers with rods of variable sections, J. Eng. Thermophys. 32 (2012) 113–116 (in Chinese).
[56] H.K. Versteeg, W. Malalasekera, An Introduction to Computational Fluid Dynamics: The Finite Volume Method, second ed., Wiley, New York, 1995.
[57] B.E. Launder, D.B. Spalding, Lectures in Mathematical Models of Turbulence, first ed., Academic Press, London, 1972.
[58] D.K. Edwards, V.E. Denny, A.F. Mills, Transfer Processes, second ed., Hemisphere, Washington, DC, 1979.
[59] E.N. Sieder, G.E. Tate, Heat transfer and pressure drop of liquids in tubes, Ind. Eng. Chem. 28 (1936) 1429–1435.
[60] H.L. Langhaar, Steady flow in the transition length of a straight tube, J. Appl. Mech. 9 (1942) 55–58.